STRESS STATE AT SOULTZ-SOUS-FORÊTS TO 5 KM DEPTH FROM WELLBORE FAILURE AND HYDRAULIC OBSERVATIONS.

Benoît Valley
Keith F. Evans

ETH Zürich – Engineering geology
ETH Hoenggerberg
Zürich, CH-8093, Switzerland
e-mail: valley@erdw.ethz.ch

ABSTRACT

Observations of breakouts and drilling-induced tension fractures (DITFs) in two 5 km deep boreholes of the European Enhanced Geothermal Project of Soultz-sous-Forêts, France have been combined with the analysis of pressure data from stimulation tests in all 3 deep wells to obtained a description of the state of stress in the granite down to 5 km depth. The orientation of the maximum horizontal stress, SHmax, in the 5 km deep reservoir is found to be N169°E±14°, in accord with previous results from the 3.5 km reservoir. Analysis of pressure at the casing shoe of the deep boreholes during stimulation permits the profile of Shmin magnitude to be extended down to 5 km depth. Finally, by combining all available information, bounds were set on the magnitude of SHmax. The result is a linear characterisation for the stress state at Soultz that is valid between depths of 1.5-5.0 km (excluding the effects of local stress heterogeneity).

INTRODUCTION

Knowledge of the state of stress is very important for the development of Enhanced Geothermal Systems (EGSs), not least because it is a primary factor influencing the reservoir response to the massive stimulation injections. Knowledge of the stress state in the 5 km deep reservoir at Soultz-sous-Forêts is largely based upon extrapolation of the characterisation defined for the shallower reservoir to 3.5 km depth. Although this has been extensively studied, some questions remain, principally with regard to the magnitude of the maximum horizontal principal stress, SHmax. This paper presents some new results that directly constrain the stress state in the deep reservoir, including the magnitude of SHmax. The constraints arise principally from analysis of breakouts and drilling-induced tension fractures (DITFs) on ultrasonic borehole wall images from two of the three wells that penetrate the deep reservoir. It is well established that these features constitute one of the best indicators of the orientation of the principal horizontal stresses. However, since they represent stress-induced failure of the wellbore, a careful analysis of the conditions of their formation allows constraints to be placed upon stress magnitudes. To obtain unique values for the two principal horizontal stress magnitudes requires that one be independently specified. Thus we analyse downhole pressure data from stimulation injections to estimate the magnitude of Shmin, and use this in the analysis of wellbore failure to constrain the magnitude of SHmax.

DESCRIPTION OF THE DATASET

The data analysed in this study stem from two of the three deep wells drilled to 5km at the Soultz-sous-Forêts geothermal project site, located in the Rhine Graben north of Strasbourg, France. The two wells, called GPK3 and GPK4, have both been drilled as deviated boreholes and reach a total true vertical depth of about 5km. GPK3 was drilled in 2002, while GPK4 was completed early in 2004. The geological section at Soultz consists of 1.4 km of Permian, Mesozoic and Cenozoic sediments underlain by a block-faulted, Hercynian age monzogranite basement. For more information about the project, refer to Dezayes (2005a).

Ultrasonic borehole images

The ultrasonic borehole televiewer images on which wellbore failure stress indicators were identified were obtained from Schlumberger Ultrasonic Borehole Imager (UBI) logs that were run with the ancillary GPIT module which provides sonde positioning and orientation information. The latter also includes two on-board temperature sensors that provide a measure of borehole temperature at the time the logs were run, which was shortly after the completion of drilling. Successful UBI logs were run in the granite section of both GPK3 and GPK4 to total depth (TD). The UBI tool provides detailed images of the ultrasonic reflectivity of the borehole wall together with borehole geometry sampled with an angular

resolution of 2°. The logging speed is chosen that a scan is made every 1 cm along hole. For detailed on measurement principle refer to Luthi (2001).

The GPK3 logs were acquired in two runs. The first run was acquired on 25th Oct. 2002 in the 12-1/4 inch section, some 5 days after the completion of drilling. This log extends throughout the 12-1/4 inch section from 1439 m MD (the casing shoe of a higher section) to 4532.6 m MD (MD denotes measured depth along hole from ground level). The images of the lowermost 13.8 m are not oriented. The second log was run on 10th Nov. 2002, some 21 days after the hole had been extended as 8-1/2 inch diameter to TD at 5103 m MD. The log covers the 8-1/2 inch section from the 12-1/4 inch casing shoe at 4558.2 m MD to 5100.8 m MD, with the lowermost 2.6 m not oriented. The images are generally of good quality with few logging artefacts. 'Key seats' (Lofts & Bourke, 1999) are visible along the entire inclined 12-1/4 section and some parts of the inclined 8-1/2 section, but they are easily identifiable and affect only a limited part of the borehole circumference.

The logs in the GPK4 borehole were also acquired in two runs that followed the drilling of the 12-1/4 inch and 8-1/2 inch sections. The log in the 12-1/4 inch was run on 15th Feb. 2004, some 15 hours after drilling, from 1421.3 to 4723.3 m MD. The log in the 8-1/2 inch section was run on 12th Apr. 2004, 18 hours after drilling operations ended, from 4730.3 to 5253.3 m MD. Images suitable for fracture geometry determination were obtained for 1445.3-4720.3 m MD and for 4757.3-5248.3 m MD. Outside these ranges, the logs are run in casing or suffer from acquisition problems.

Description of wellbore failure

Breakouts or drilling-induced tension fractures occur when the local value of tangent compression or tension respectively at the borehole wall exceeds the rock strength. Breakouts are typically manifest as pairs of diametrically-opposite spall zones that extend along the borehole axis. In the simple case of a vertical borehole penetrating a rock mass in which one principal stress is vertical, breakouts, if they occur, indicate the orientation of the Shmin (Bell & Gough, 1979).

Drilling induced tension fractures (DITFs) form where cooling of the borehole wall by circulation of mud during drilling results in a net tangent stress distribution about the hole that is sufficiently tensile at some point to produce failure. The net tangent stress is the sum of a tensile cooling component, which is axially-symmetric, and the natural wellbore stress concentration arising from the 'far-field' stresses, which are not necessarily axially-symmetric and may be everywhere compressive. In the case of a

vertical borehole penetrating a medium in which one principal stress is also vertical, the least compressive value of the circumferential stress variation about the borehole due to the far field stresses occurs in the direction of SHmax. Thus, it is in this direction that the greatest tension develops and a pair of diametrically-opposite DITFs form. If the borehole axis is aligned with a principal stress, they will be axial, and denoted as A-DITFs. However, in the case where the borehole axis is not aligned with a principal axis, the criterion for tensile failure might still be met but then DITFs will tend to form as a stack of en-echelon induced fractures, denoted E-DITFs. The relationship between the induced fracture geometry and the in-situ stress orientations and magnitudes in this case is not as simple as in the aligned case.

The stress-controlled wellbore failure features were identified and described as follows. First, borehole intervals affected by either breakouts (BOs), axial drilling induced tension fractures (A-DITFs) or "en echelon" drilling induced tension fractures (E-DITFs) were identified. Then, for breakouts and A-DITFs the mean orientation of features was determined over successive 0.5 m depth windows. For E-DITFs the mean orientations (strike) of the best-fitting plane for each fracture pair were chosen. In all cases, the confidence of the identification was recorded by assigning an index ranging between 1 and 3, corresponding to low and high confidence respectively.

Similar counts of features were obtained for both boreholes. About 10% of the logged borehole lengths are affected by breakouts, 10% by A-DITFs, and 7% by E-DITFs. The orientation distributions with depth of the breakouts and DITFs in GPK3 are shown in Figure 1. The corresponding plot for GPK4 is given in Figure 2.

INTERPRETATION OF THE WELLBORE FAILURE TO CONSTRAIN STRESS STATE

Principal stress orientation

The inclination of the boreholes is shown in the left frames of Figures 1 and 2. The occurrence of A-DITFs along the vertical borehole sections suggests that one principal stress is locally vertical, whereas the presence of E-DITFs along such sections indicates a local deviation of the 'most vertical' principal stress from true verticality. Note that the E-DITFs are always fairly steep and deviate both to the east and to the west so that their mean orientation is about vertical. This suggests that one principal stress is, on average, vertical, with localised deviations from verticality indicating zones of stress heterogeneity. Thus, for the stress characterisation we take one principle stress as vertical and so only the
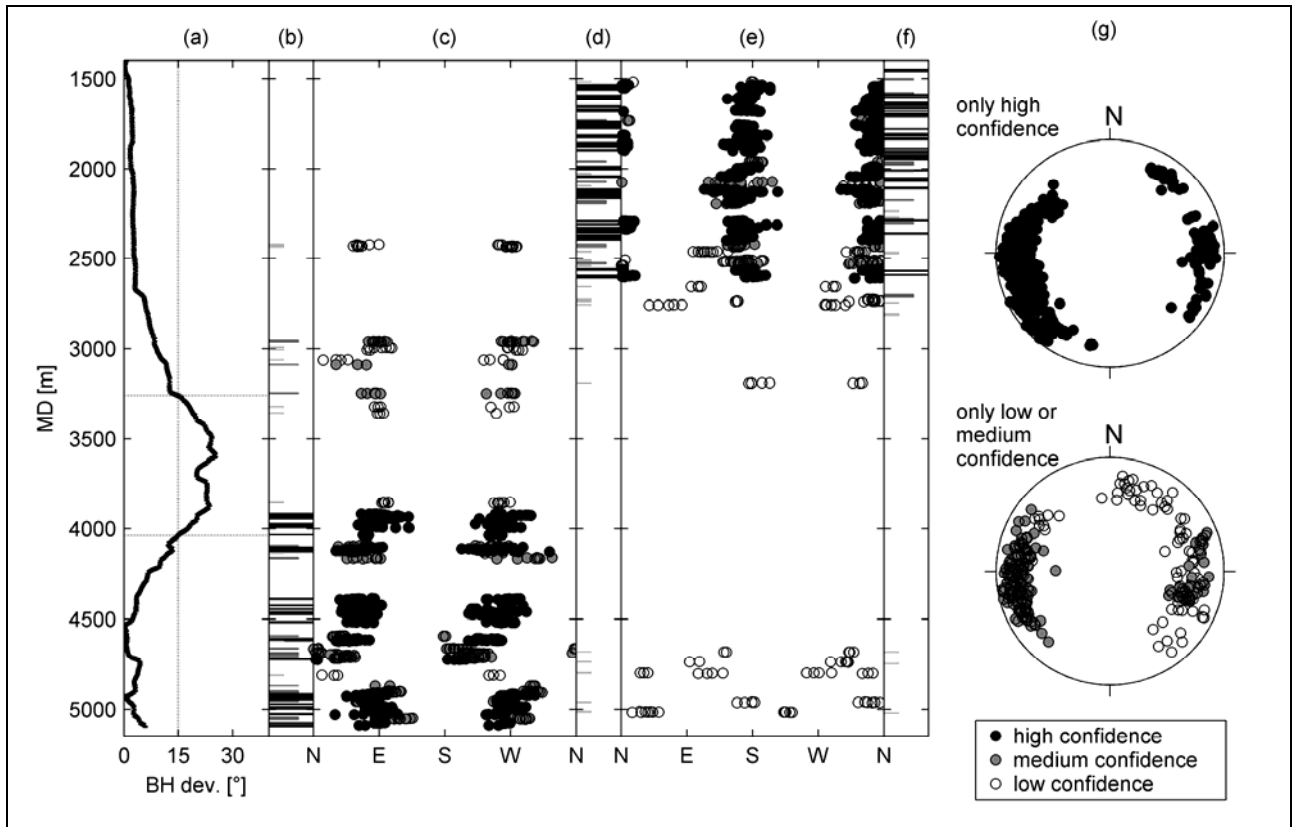
Figure 1: Summary of wellbore failure observations in the borehole GPK3. a) Borehole deviation from verticality. b) Breakout intervals. c) Breakout orientation. d) A-DITF intervals. e) A-DIFT strike directions. f) E-DITF intervals. g) Stereographic projections of poles to E-DITF planes (lower hemisphere, equal area).
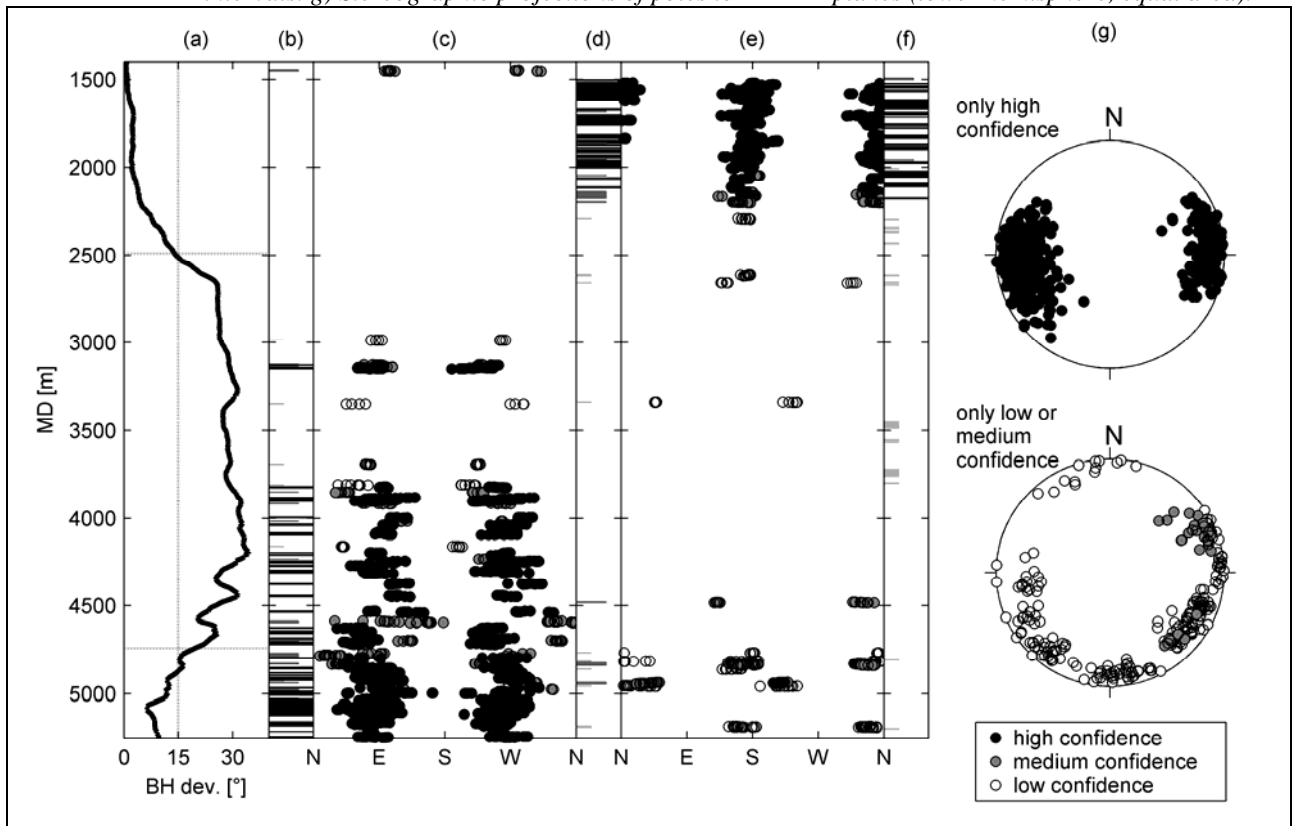

Figure 2: Summary of wellbore failure observations in the borehole GPK4. See Figure 1 caption for explanation.
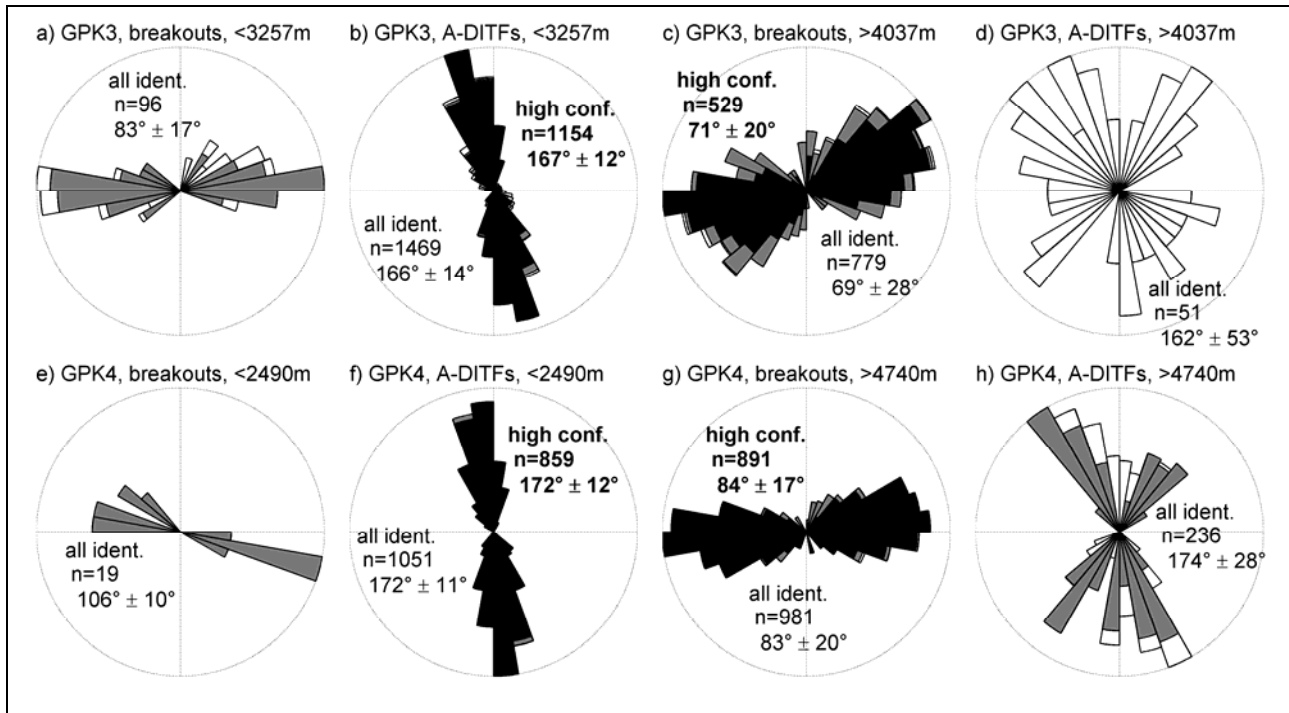
Figure 3: Circular histograms of breakout and A-DITF orientations along sub-vertical sections of GPK3 and GPK4. Unfilled denotes low confidence data; grey denotes medium confidence data, and black is for high confidence data. The circular mean direction and single standard deviation are given.

direction of the maximum horizontal stress has to be ascertained to fully characterise principal stress orientation.

For the vertical borehole sections, the wellbore failure features provide a direct measure of the horizontal stress orientations: the breakouts denote the Shmin-orientation, and the DITFs the SHmax-orientation. For the purpose of the analysis we consider borehole sections that lie within 15° of vertical as being essentially vertical. For GPK3, this excludes from the analysis the section between 3257 m and 4037 m MD. Above 3257m MD, borehole failure is dominated by numerous A-DITFs, with only a few medium- to low-confidence identifications of breakouts. The high-confidence A-DITFs show a preferred orientation in this section of 167.3° ± 12.1° (see histogram of Figure 3b), a result that does not significantly change by including medium- and low-confidence estimates. The orientation of the medium- and low-confidence breakouts is found to be 83.4° ± 17.3° (Figure 3a), which is approximately 90° rotated from the mean A-DITF orientation, as would be expected if the identifications were correct. This indicates that some, albeit few, breakouts do indeed occur above 3257 m MD. In contrast, the lower sub-vertical section of the borehole, below 4037 m MD, is dominated by numerous breakouts with only a few low-confidence A-DITFs present. The high confidence breakouts have an orientation of 71.3° ± 20.3°. The A-DITFs have no clear preferred

orientation, and since they are all low-confidence, are possibly erroneous identifications.

A similar distribution of wellbore failure features is seen in GPK4, which is sub-vertical above 2490 m MD and below 4740 m MD. Many A-DITFs are found in the upper sub-vertical part, whereas only one medium confidence breakout is present. High confidence A-DITFs for this upper section show a clear preferential orientation of 172.2° ± 11.8°. Below 4740 m MD, breakouts dominate with a few medium-to-low confidence A-DITFs. The high-quality breakouts have a strong preferred orientation of 83.8° ± 17° (see histogram in Figure 3g). The medium-to-low confidence A-DITFs are oriented 173.9° ± 28.0°, and are thus 90° from the breakouts. This suggests that at least some of the identified A-DITFs are real.

SHmax-orientation estimates obtained from the mean direction of the high-quality A-DITFs in the upper sub-vertical sections of GPK3 (167°±12°) and GPK4 (172°±12°) are consistent with the results of previous analyses from the wells in the shallow reservoir (0°±20°). In the lower sub-vertical sections of GPK3 & 4, the high-quality breakout identifications indicate an SHmax-orientation for the deeper reservoir of 162°±20° and 174°±17° respectively, which is not significantly different from the SHmax-orientation in the shallow reservoir (see synthesis in Cornet et al., 2007). Taking an average

of all estimates from GPK3 and GPK4 by weighting each value by the length of borehole considered in the study yields a mean orientation for SHmax at the Soultz site from 1.4 km to 5 km depth of 169°±14°.

Natural formation pressure

The natural formation pressure is required for computations that involve effective stresses. The value used here is based on brine density profiles given in Evans, et al. (1992) and is:

$$Pp = 0.9 + 9.8 \ z[km] \tag{1}$$

Vertical stress magnitude

Since the evidence indicates that on average one principal stress is vertical, its magnitude can be taken as the integrated overburden as estimated from density determinations from either logs or tests on core samples. The density profile from 898 m to 3.6 km is reasonably well-constrained from density logs and tests of core samples. Klee and Rummel (1999) propose a Sv profile based on a density of 2.66 gm/cc from core tests. However, this is almost certainly an overestimate as it excludes the contribution of the relatively low densities found in alteration zones. Wireline density logs indicate a mean density for the granite to 3.6 km of 2.63 gm/cc. Moreover, comparison of the density of a core sample taken in GPK1 at 3524 m with the values registered on the density log in the vicinity showed excellent agreement, the log values being at most 0.015 gm/cc too low. Thus we regard the estimates from the density log as valid.

Above 898 m there is no density log from the Soultz site. A compilation by BRGM of density estimates from unspecified wireline logs run in unspecified boreholes in the Rhine Graben indicates values that show large scatter and differ significantly from the density log run in Soultz well GPK1 between 898 m and 1377 m. Thus, this compilation cannot be used to precisely estimate the density profile. However, a trend towards significantly lower densities in the upper 500 m is clearly defined in the compilation, presumably reflecting increasing porosity due to incomplete compaction and diagenesis. In view of these considerations, the density profile in the sedimentary section was estimated using the GPK1 density log between 1377 and 898 m, and the lithological composition of the sedimentary units above. A gradual upward reduction in density in the Cenozoic sediments above 594 m to a value of 2.0 gm/cc at surface was applied to simulate the effects of increasing porosity. The resulting mean density of the sedimentary section was found to be 2.50 gm/cc, in agreement with the value given by Heinemann-Glutsch (1994). Below 3.6 km, there is no published information on the density of the granite, and thus we use the value of 2.6 gm/cc that is valid for the granite

above. This is somewhat questionable below about 4500 m TVD where petrological studies indicate a change in the composition of the granite (Dezayes, 2005b).

Drawing these considerations together, we conclude that the currently available data indicate that the vertical stress profile in the granite is given by:

$$Sv = -1.30 + 25.50 \ z[km] \tag{2}$$

where we estimate the uncertainty level is approximately ±2 MPa.

Minimum horizontal stress magnitude

Down to 3.5km, the magnitude of Shmin is constrained by five small-volume hydraulic tests on pre-existing fractures in the depth range 1450-1990 m (Rummel and Baumgärtner, 1991), and a further four tests on induced hydrofractures in the depth range 2190-3510 m (Klee and Rummel, 1993). These data were fitted by Heinemann-Glutsch (1994) to constrain her Shmin profile (often mistakenly accredited to Klee and Rummel (1993) who actually propose a different profile in their paper based on tests above 2000 m). Evans (2005) best fits to the same data but without the lowermost point at 3508 m, which was almost certainly conducted in a zone of perturbed stress. Cornet & Bérard, (2003) discounted all small volume tests and claimed that a better Shmin estimate was given by the maximum pressures of large-volume, relatively high-rate injections where the jacking pressure is reached. In such cases they proposed that the maximum pressure at the top of the injection interval equals Shmin at that depth, an assumption that ignores near-wellbore pressure drops and poro-elastic perturbations of the ambient stress (Evans, 2005). They based their Shmin profile on two injection tests at 2000 and 2850 m, and state the uncertainty as ±3.5 MPa.

For the deep reservoir, no formal, hydraulic stress tests have been conducted below 3.5 km from which the magnitude of Shmin could be estimated. Thus, we follow Cornet and Bérard (2003) and assume that the maximum pressure attained during the stimulation injections provides a direct measure of Shmin at the depth of the casing shoe. This approach must be considered as tentative since it assumes the following conditions are met:

1. The maximum pressure attained during the test is controlled by jacking and not shearing.
2. Near-wellbore pressure drops (i.e. entrance losses) due to the focussing of flow are negligible.
3. The minimum stress prevailing at the time of maximum pressure reflects the ambient stress and is not elevated by poro-elastic effects.

These conditions appear to have been met for the large injections into the shallower reservoirs at 2.0

and 3.0 km, since the suggested Shmin profile of Cornet and Bérard (2003), which is based on maximum pressures during large volume injections, does not differ greatly from that determined from the small-volume injections. Violation of assumption 1 would result in underestimation of the ambient minimum stress, whereas 2 and 3 would result in overestimates. The data describing the maximum pressures inferred at the casing shoe during stimulation injections of the three wells of the 5 km reservoir are listed in Table 1 and are plotted in Figure 4. Only estimates derived from downhole pressure measurements are listed. It is evident that all data show pressure-limiting behaviour. The three datapoints from the 03May27 stimulation of GPK3 are from a sequence when the flow rate was stepped from 50 l/s to 70 l/s for 2 hrs and then back to 50 l/s. The small, reversible changes in pressure that accompanied the flow rate steps indicates that jacking was occurring, as required for the Shmin estimation procedure to be valid.

The resulting estimates of Shmin are plotted as a function of depth in Figure 4, together with estimates from small-volume tests. In fitting the data with a linear trend we used only estimates obtained from large-volume injection tests because these are less sensitive to local stress heterogeneities. The Shmin estimates fall closely on a linear trend, with the exception of the data points for GPK2 which are too low by about 4 MPa. It is noteworthy that pressure was continuing to slowly increase at the end of this stimulation. This can be interpreted as indicating that the jacking pressure was not reached, although other explanations are possible. Because of this complexity, the GPK2 injection pressures were excluded from the fitting process. The resulting best-fit linear trend obtained from the casing-shoe injection pressures of the two GPK1 injections, the GPK3 and 4 injections is given by:

$$Shmin = -1.78 + 14.06\ z[km] \qquad (3)$$

Maximal horizontal stress magnitude

The commonly-used profile of SHmax for the Soultz site is derived from hydrofracture test data using the 're-opening method' (Klee and Rummel, 1993). Several authors have shown that this method yields

invalid SHmax estimates (Ito, et al., 1999; Rutqvist, et al., 2000), particularly in deep holes, and this has led others to discount them (e.g. Cornet & Bérard, 2003; Evans, 2005). A semi-quantitative constraint on SHmax stems from the observation that focal mechanisms show a mix of normal and strike slip faulting, suggesting that SHmax is not greatly different from Sv. Both Cornet & Bérard (2003) and Evans (2005) adopt this equality as a working hypothesis. An extreme lower bound on SHmax is
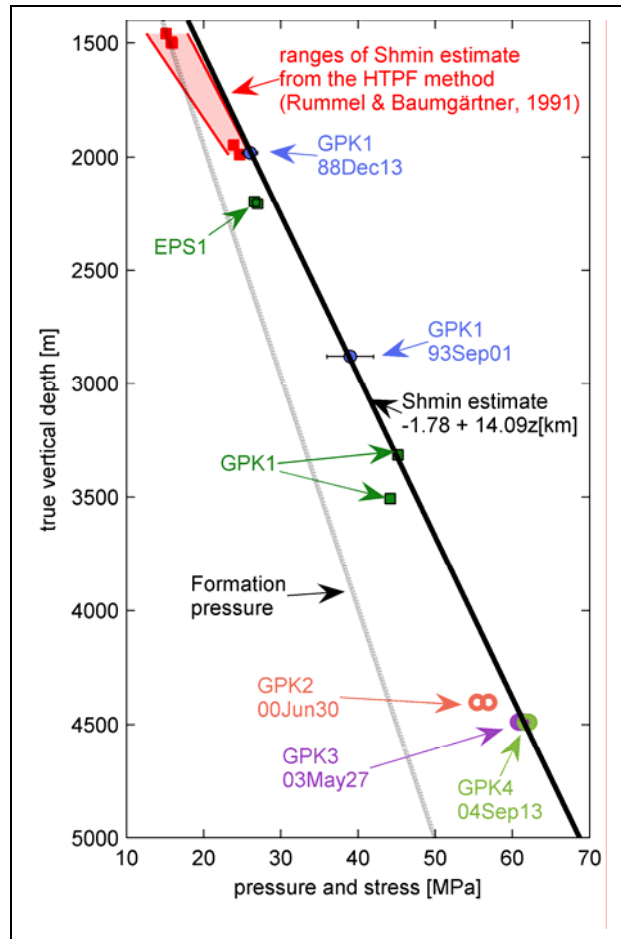

Figure 4: Estimates of the Shmin from small-volume injection tests (squares) and large-volume injection tests (circles). See text for details.

Table 1: Maximum pressures recorded at the casing shoe during the stimulation injections of the three deep wells. The data denote the pressures prevailing at the end of injection stages with different flowrates.

Borehole	Injection test ID	Depth of casing shoe [m TVD from ground]	Max. pressure at casing shoe [MPa]	Flow rate at max. pressure [l/s]
GPK2	00JUN30	4402	55.4	31
GPK2	00JUN30	4402	56.9	50
GPK3	03May27	4488	60.8	50
GPK3	03May27	4488	61.5	70
GPK3	03May27	4488	61.2	50
GPK4	04SEP13	4489	62.1	30
GPK4	04SEP13	4489	61.7	40

that it must be greater than Shmin by definition. An upper bound on SHmax is obtained by assuming that the strength of fractured rock masses is limited by thefrictional strength of optimally oriented fractures (Brace and Kohlstedt, 1980). The worldwide crustal stress dataset supports this view and indicates an upper limit on rock mass strength can be represented by a Coulomb friction criterion with a friction coefficient of 1.0 and zero cohesion. Evans (2005) showed that this constraint imposes an upper limit on SHmax of 1.21·Sv.

The observed partitioning of borehole failure mechanisms to different depth regimes in the deep Soultz boreholes allows a refinement of the SHmax profile. Specifically, tensile failure in the form of DITFs is seen to dominate at shallow depth, and compressive failure in the form of breakouts below. Since the UBI logs from which the breakouts and DITFs were identified were run before any injections had been conducted, the failure must have occurred either during drilling or shortly afterwards. In general, the total stresses about a wellbore can be considered to result from the superposition of four components: 1) the stress concentration developed around an empty wellbore due to the far-field stresses applied to the medium with uniform pore pressure; 2) the stresses generated by the wellbore fluid pressure; 3) the stresses arising from a perturbation of pore pressure about the well, and 4) the stresses arising from a perturbation of temperature about the well. Components 1 and 2 are always present. They represent the tangent stresses prevailing long after drilling, when the well has reached thermal and hydraulic equilibrium with the surroundings. In contrast, the conditions just after drilling (i.e. when the UBI logs were acquired) include the perturbing stress components 3 and 4 activated in tension by the cooling and overpressuring effects of the drilling mud. The latter is believed to be small for the holes in question since the annulus pressure was maintained at near-hydrostatic conditions. Hence it will be neglected. In this paper we consider components 1,2 and 4, and use data from hydraulic tests and temperature logs to constrain SHmax.

Analysis of the breakouts requires a compressive strength criterion. Uniaxial compressive tests were conducted on ten samples of unaltered Soultz granite, and yielded values of 100-130 MPa. Several authors (Wiebols and Cook, 1968; Haimson and Chang, 2005; Al-Ajmi and Zimmermann, 2006; Haimson, 2007) have proposed failure criteria that attempt to take into account the triaxial stress state at the borehole wall, although there is currently no consensus as to which is the most appropriate. We assume the appropriate strength is given directly by the UCS. Although it is true that higher strength estimates would have been obtained had the tests been conducted under the confining conditions that

prevail at borehole wall, there are other issues that should be born in mind when considering whether laboratory values of strength derived from tests on cores are representative of in-situ values. Firstly, there is the question of microcracking induced by stress relief. Both cores and borehole wall have experienced complex stress paths when being drilled. Whilst these paths are not identical, both involve stress relief to some extent, and both will result in damage and strength reduction in comparison to that of *in-situ* rock remote from the wellbore (Diederichs, 2004; Martin, 1994). Thus, the reduction in strength of the core samples mimics that of the borehole wall to some degree. A second consideration is that stress corrosion cracking will serve to reduce the strength of the borehole wall on timescales which are long compared to the laboratory tests. This weakening of the wall rock will be promoted by the high in-situ temperature and the reactive nature of the pore fluid. In summary, there are competing effects that make it is difficult to decide whether UCS tests conducted in the laboratory are higher or lower than the strength of the rock at the borehole wall under *in-situ* conditions. The breakout analysis also includes an effective stress law for compressive failure with a coefficient of 1.0, as found by Brace and Martin (1968) to be valid even for very low-porosity crystalline rocks.

The results of the analysis for GPK4 are summarised in Figure 5. No high-confidence breakouts are identified above 3000 m (Figure 5a). Below 3000 m, breakouts are sparsely distributed until 3670 m TVD when the density increases markedly. Figure 5b shows the profile of maximum tangent effective stress obtained for a Shmin profile given by eqn 3, and a range of SHmax profiles. The profiles are primarily governed by stress-perturbing components 1 and 2 noted above. However, there is also potentially a component from thermal stress since the well had not warmed up to thermal equilibrium at the time the UBI log was run. Since the effect of the thermal stress is to generate a tensile stress it will serve to inhibit breakout formation. Thus, the analysis of whether conditions for breakout formation are met at a given depth requires knowledge of the hottest temperature the borehole has reached at that depth since its time of drilling up to the time of the UBI log. This is difficult to estimate because of the complicated circulation history of the well during drilling, and the cooling circulations performed before logging. Thus, we used an upper limit on the thermal stress from the temperature profile indicated by the GPIT sonde. This yields the lower bounds on the tangent stress shown in the dashed curves of Figure 5b. The dotted curve denotes the upper bound on tangent stress for the case SHmax = 1.2Sv, and is obtained by setting the thermal stress to zero. Evidently, the inclusion of thermal stress has little effect on the analysis. The grey band in Figure 5b
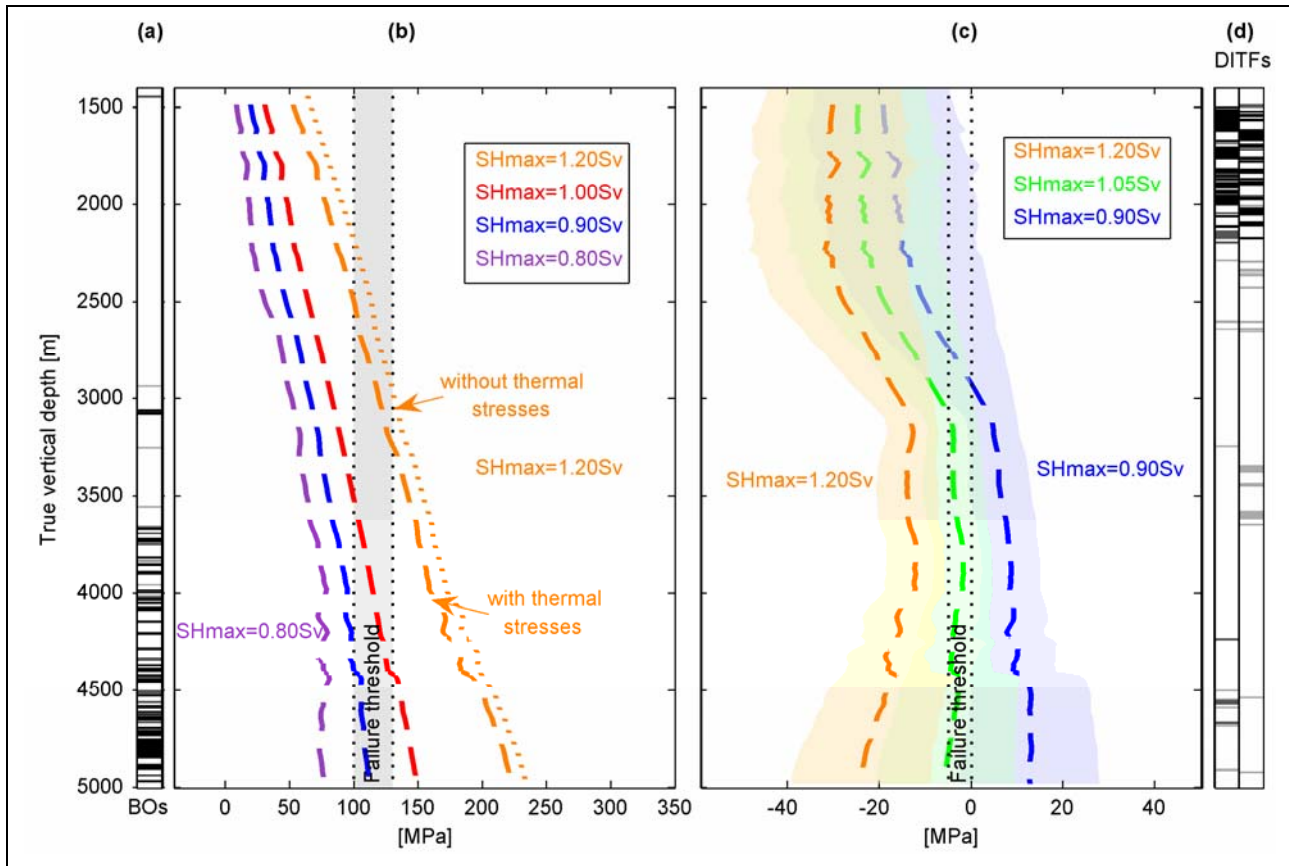
Figure 5: Constraints imposed on SHmax-magnitude by the observed wellbore failure in GPK4 . a) Breakout locations. Black bars are for high confidence, grey bars for medium confidence and light gray bars for low confidence. b) Maximum tangent effective stress for compressive failure. The coefficient in the effective stress law was taken as 1.0. The dashed profiles include a thermal hoop stress computed from the temperature profile at the time of the UBI logs, and the dotted profile is without a thermal hoop stress component. The vertical band denotes the compressive failure threshold derived from UCS measurements. c) Minimum tangent effective stress for tensile failure including an effective law with a coefficient of 0.0 and thermal hoop stress. Light coloured areas around the profiles represent uncertainty on the thermal hoop stress estimate. d) DITFs locations with same confidence rating that for the breakouts. See text for further discussion.

denotes the threshold tangent stress for compressive failure. The dashed curves indicate that SHmax must be greater than or equal to 0.9·Sv in order to reproduce the onset depth of breakouts at 3670 m.

The distribution of DITFs along GPK4 is shown in Figure 5d. Tensile failure of GPK4 is almost continuous down to 2180 m TVD, whereas below that depth it is sporadic and highly localised. To constrain SHmax from this distribution, profiles of minimum tangent stress were generated using the Shmin profile of eqn. 3 and a range of values of SHmax. Estimation of the component 4 (thermal stress) for the case of DITFs requires that the coolest temperature seen by the borehole wall be estimated at each depth. For this we used spot measurements of fluid temperature at the bit recorded by a 'measurement-while-drilling' system together with temperature measured within the GPIT tool during

the UBI logs. These were run 12-15 hours after the end of drilling operations. The resulting profiles of minimum tangent stress are shown in Figure 5c. The coloured zones around each profile denote the potential error arising from the uncertainty in the true profile of 'coolest temperature' obtained from the data. The thermal stress component to the tangent stress profiles is found to range from -17.1 MPa at 3160 m TVD to -31.3 MPa at 2235 m TVD.

To determine whether the computed minimum tangent stress at the borehole wall is sufficient to generate a DITF, a failure criterion in tension is required that includes an effective law. No laboratory measurements of the tensile strength of Soultz granite are available. A review of the literature suggests values for intact specimens will probably be of the order of 10-20 MPa. However, in-situ values will be less than this – perhaps as low as a few MPa – owing

to microcrack growth. Indeed, many practitioners adopt a value of zero when considering similar borehole stability problems (e.g. Brudy and Zoback, 1993). In view of this, tensile strength will be considered to range between 0 and 5 MPa. There is considerable uncertainty regarding the value of the coefficient in the effective stress law for tensile failure that is appropriate for low-porosity crystalline rocks. Laboratory studies found a value of unity (Jaeger, 1963; Jaeger and Cooke, 1963; Schmitt and Zoback, 1992), except possibly when the loading rate is very high and fluid pressure equilibrium is not maintained. This may be relevant for special problems like impacts or explosion but probably not for borehole failure. Thus, our starting hypothesis is that this coefficient is equal to 1.0. However, it was found that taking a value of 1.0 led to tensile failure initiation along the entire length of the hole for all considered values of SHmax. Results that are in accord with observation can only be obtained by significantly reducing the coefficient. The minimum tangent stress curves in Figure 5c can be considered to be effective stresses for the extreme case where the coefficient is zero. These curves indicate that to prevent tensile failure in the lower half of the well it is necessary for SHmax to be at most 1.05·Sv. Thus, the breakouts and DITFs together constrain the profile of SHmax to be 0.90·Sv ≤ SHmax ≤ 1.05·Sv.

Conclusions

A detailed description and analysis of stress-induced wellbore failure in the form of breakouts and drilling induced tension fractures was performed for two of the 5 km depth borehole of the European Enhanced Geothermal Project of Soultz-sous-Forêts. When combined with an estimate of Shmin magnitude from the maximum pressures developed at the casing shoes of the wells during major injections, the wellbore failure observations impose constraints on the magnitude of SHmax, as well as its direction. The collective analysis suggests the following stress characterisation for Soultz that is valid between depths of 1.5-5.0 km (excluding the effects of local stress heterogeneity):

SHmax orientation is N169°E±14°
Sv = -1.30 + 25.50 z[km]
Shmin= -1.78 + 14.06 z[km]
- 1.17+22.95z[km] ≤ SHmax < -1.37+26.78z[km]

A further result of the analysis is that the coefficient of the effective stress law for tensile failure is significantly less than unity.

ACKNOWLEDGEMENTS

REFERENCES

Al-Ajmi, A. M., and R. W. Zimmermann (2006), Stability of vertical boreholes using the Mogi-Coulomb failure criterion, *International Journal of Rock Mechanics and Mining Science*, **43**, p. 1200-1211.

Bell, J. S., and D. I. Gough (1979), Northeast-southwest compressive stress in Alberta: Evidence from oil wells, *Earth and Planetary Science Letters*, **45**, 2, p. 475-482.

Brace, W. F. and Kohlstedt D. L. (1980), Limits on lithospheric stress imposed by laboratory experiments, *Journal of Geophysical Research*, **85**, p. 6248-6252.

Brace, W. F., and R. J. Martin (1968), A test of the law of effective stress for crystalline rock of low porosity, *International Journal of Rock Mechanics and Mining Science*, **5**, p. 415-426.

Brudy, M., and M. D. Zoback (1993), Compressive and Tensile failure of boreholes arbitrarily-inclined to principal stress axes: application to the KTB boreholes, Germany, *International Journal of Rock Mechanics, Mining Science and Geomechanics Abstracts*, **30**, p. 1035-1038.

Cornet, F. H., and T. Bérard (2003), A case example of integrated stress profile evaluation, paper presented at 3rd International Symposium on Rock stress, Balkema, Kumamoto.

Cornet, F. H., Bérard, T. and S. Bourouis (2007), How close to failure is natural granite rock mass at 5 km depth ?, *International Journal of Rock Mechanics and Mining Science*, **44**, p. 47-66.

Dezayes, C., Gentier, S. and A. Genter (2005a), Deep Geothermal Energy in Western Europe: The Soultz Project, Public Report RP-54227-FR, 51 pp, BRGM, Orléans.

Dezayes, C., Chevremont, P., Tourlière, B., Homeier G. and A. Genter (2005b), Geological study of the GPK4 HFR borehole and correlation with the GPK3 borehole (Soultz-sous-Forêts, France), Public Report RP-53697-FR, 97 pp, BRGM, Orléans.

Diederichs, M. S., Kaiser, P. K. and E. Eberhardt (2004), Damage initiation and propagation in hard rock during tunnelling and influence of near-face

stress rotation, *International Journal of Rock Mechanics and Mining Science*, **41**, p. 785-812.

Evans, K. F., Kohl, T., Hopkirk, R. J. and L. Rybach (1992), Modelling of energy production from Hot Dry Rock systems, Final Report, Bundesamt für Bildung und Wissenschaft.

Evans, K. F. (2005), Permeability creation and damage due to massive fluid injections into granite at 3.5 km at Soultz: 2. Critical stress and fracture strength, *Journal of Geophysical Research*, **110**,

Haimson, B., and C. Chang (2005), Brittle fracture in two crystalline rocks under true triaxial compressive stresses., in *Petrophysical properties of crystalline rocks.*, edited by P. K. Harvey, et al., pp. 47-59, Geological Society Special Publications, London.

Haimson, B. (2007), Micromechanisms of borehole instability leading to breakouts in rocks, *International Journal of Rock Mechanics and Mining Science*, **44**, p. 157-173.

Heinemann-Glutsch, B., (1994), Results of scientific investigations at the HDR test site, Soultz-sous-Forêts, Alsace, Socomine, BP 39, Route de Kutzenhausen, F-67250 Soultz sous Forets., France

Ito, T., Evans, K. F., Kawai, K. and K. Hayashi (1999), Hydraulic fracture reopening pressure and the estimation of maximum horizontal stress, *International Journal of Rock Mechanics and Mining Science*, **36**, p. 811-826.

Jaeger, J. C. (1963), Extension Failures in Rocks subject to fluid Pressure, *Journal of Geophysical Research*, **68**, p. 6066-6067.

Jaeger, J. C., and N. G. W. Cooke (1963), Pinching-off and disking in rocks, *Journal of Geophysical Research*, **68**, p. 1759-1765.

Lofts, J. C., and L. T. Bourke (1999), The recognition of artefacts from acoustic and resistivity borehole image devices, in *Borehole Imaging: applications and case histories*, edited by M. A. Lovell, et al., p. 59-76, Geological Society, London.

Klee, G., and F. Rummel (1993), Hydrofrac stress data for the European HDR research project test site Soultz-sous-Forêts, *International Journal of Rock Mechanics, Mining Science and Geomechanics Abstracts*, **30**, p. 973-976.

Luthi, S. M. (2001), Geological well logs : their use in reservoir modeling, 373 pp., Springer.

Martin, C. D., and B. Stimpson (1994), The effect of sample disturbance on laboratory properties of Lac du Bonnet granite, *Canadian Geotechnical Journal*, **31**, p. 692-702.

Rummel, F., and J. Baumgärtner (1991), Hydraulic fracturing stress meausrments in the GPK1 borehole, Soultz-sous-Forêts, *Geothermal Science and Technology*, **3**, 119-148.

Rutqvist, J., Tsang, C. F. and O. Stephansson (2000), Uncertainty in the maximum principal stress estimated from hydraulic fracturing measurements due to the presence of the induced fracture, *International Journal of Rock Mechanics and Mining Science*, **37**, p. 107-120.

Schmitt, D. R., and M. D. Zoback (1992), Diminished pore pressure in low-porosity crystalline rock under tensional failure; apparent strengthening by dilatancy., *journal of Geophysical Research*, **97**, p. 273-288.

Wiebols, G. A., and N. G. W. Cook (1968), An energy criterion for the strength of rock in polyaxial compression, *International Journal of Rock Mechanics and Mining Science*, **5**, 6, p. 529-549.